THE JOURNAL OF PHYSICAL CHEMISTRY B

Article

pubs.acs.org/JPCB

Odd or Even? Monolayer Domain Size Depends on Diyne Position in Alkadiynylanthracenes

Yi Xue,[†] Min Kyoung Kim, Tereza Pašková,[‡] and Matthew B. Zimmt*

Department of Chemistry, Brown University, Providence, Rhode Island 02912, United States

Supporting Information

ABSTRACT: 1,5-(Alkadiynyl)anthracenes self-assemble single component and multicomponent monolayers at the solution−HOPG interface. An alkadiynyl chain's kinked shape constrains the molecular structures with which it can close-pack. This affords rudimentary molecular recognition that has been used to direct self-assembly of 1-D patterned, multicomponent monolayers. The unit cell building blocks of single- and multicomponent alkadiynylanthracene monolayers repeat with high fidelity for 100s of nanometers along the side chain direction. Unit cell repeat fidelity along the orthogonal, anthracene column direction of the monolayer depends on diyne location within the side chain; even-position diyne side chains produce high fidelity of unit cell repeats and wider domain widths along the anthracene columns, whereas odd-position diyne side chains produce more frequent domain interfaces that disrupt the anthracene columns. Alkadiynylanthracene monolayers may be viewed as stacks of 1-D molecular tapes. 1-D tape molecular composition, sequence, and intratape side chain alignment are dictated by shape complementarity of the kinked alkadiynyl side chains. Stacking alignments of adjacent 1-D tapes are controlled by shape matching of tape peripheries and determine repeat fidelity along the anthracene columns. Tapes stacked with a constant intertape alignment comprise crystalline domains that repeat along the anthracene columns. The 1-D tapes formed by anthracenes with odd-position diynes have triangle wave peripheries that close-pack in multiple stacking alignments. This reduces unit cell repeat fidelity and decreases the widths of crystalline domains along the anthracene columns. Even-position diyne side chains form 1-D tapes with trapezoid wave peripheries that close-pack in only one stacking alignment. This generates higher stacking fidelity, larger domain widths, and fewer domain interfaces along the anthracene columns of even-position diyne monolayers. Even- and odd-position diyne monolayers exhibit comparable densities of interfaces between enantiotopic domains and between domains aligned along different graphite symmetry axes. These interfaces likely arise through collisions of independently nucleated/growing domains and persist for lack of kinetically competent pathways that interconvert or merge the domains.

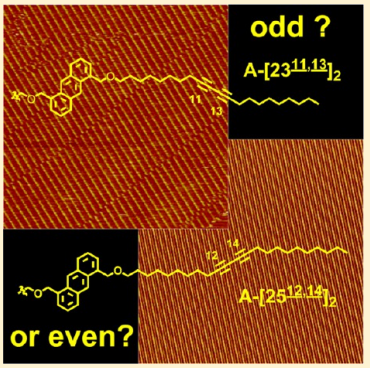

INTRODUCTION

Self-assembly in nature produces complex structures spanning length scales from submicrometer to meters with remarkable reproducibility.[1,2] The functions of natural systems depend on precise placements of multiple components.[3] Increased understanding of self-assembly, including in 2-D, has fostered progress toward a priori design of molecularly patterned and functional self-assembly systems.[4−6] One of the enduring challenges, known since some of the earliest 2D self-assembly studies, is that subtle changes to component structures can produce very different local packing and significant differences in long-range order.[7,8] Recent studies have reported designed multicomponent systems that self-assemble structurally patterned monolayers.[4−6,9−16] Local order in these assemblies, that is, the identities and placements of neighboring components on length scales of a few 10s of nanometers, can be precise and regular, producing crystalline domains. However, long-range order tends to be less well controlled, with the cumulative impact of defects and interfaces destroying structural regularity on length scales exceeding 100s of nanometers.

Two recent reports described multicomponent systems that self-assemble compositionally patterned, two-component (**1** and **2**) or four-component (**3**−**6**) alkadiynylanthracene monolayers at the solution−HOPG interface (Chart 1).[17,18] Composition variation along the side chain direction of these monolayers is determined with high fidelity on length scales exceeding 100s of nanometers by matching of shape complementary, kinked alkadiynyl side chains. Along the orthogonal monolayer direction, i.e., parallel to the anthracene columns, the design intends no variation of composition or packing alignment. In practice, this intended homogeneous packing along the anthracene columns is disrupted by packing misalignments in both the two- and four-component monolayers. These disruptions occur in long stretches of adjacent anthracene columns and comprise interfaces between domains. Each domain exhibits the intended packing along

Special Issue: Michael D. Fayer Festschrift

Received: August 22, 2013
Revised: September 24, 2013
Published: September 24, 2013

Chart 1

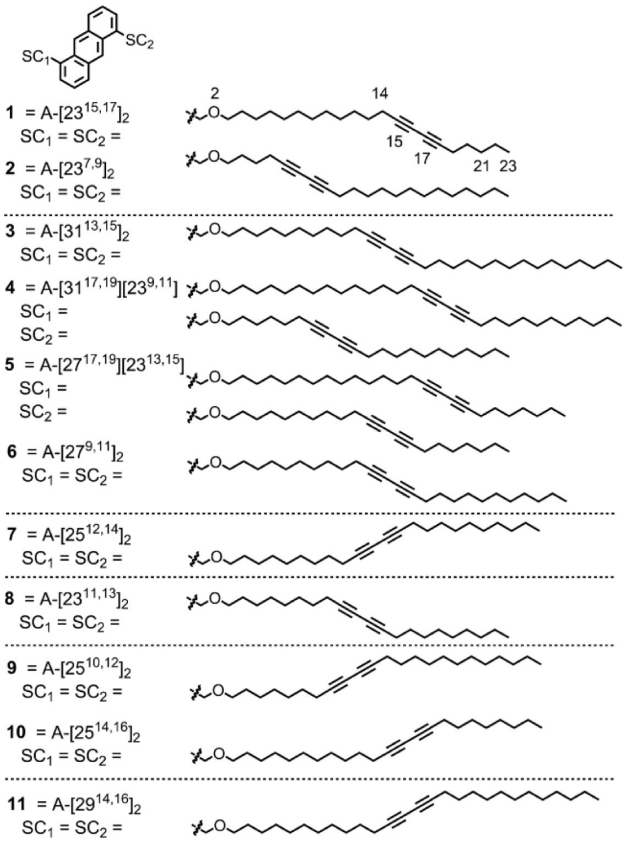

both the side chain direction and along the orthogonal, anthracene column direction. However, the domain widths parallel to the anthracene columns usually do not exceed 30–60 nm.

In contrast to the frequent domain interfaces observed within the multicomponent monolayers described above, domain interfaces are much less common in the single component monolayers self-assembled by alkadiynylanthracene **7**. These alkadiynylanthracene self-assembly systems differ in two structural elements: (i) multicomponent (**1**–**6**) versus single component (**7**) and (ii) odd (**1**–**6**) versus even (**7**) side chain location of the diyne groups. To ascertain whether the density of domain interfaces within alkadiynylanthracene monolayers relates to these or other structural elements, areal densities of the three most common domain interfaces were determined in drop-cast one-component (**8**, **7**, **11**) and two-component (**1**, **2**, **9**, **10**) monolayers assembled from odd- or from even-position diyne components. Component misalignments described as slip interfaces are the dominant domain boundaries observed in monolayers assembled from odd-position diyne side chain components but are not observed in monolayers assembled from components with even-position diyne side chains. Areal densities of the two other domain interfaces, enantio-slip and 120° interfaces, are weakly dependent on the side chain diyne location and on the number of diyne components in the monolayer. Molecular mechanics simulations and analyses of component packing energies reveal substantially lower cost to self-assemble slip interfaces in systems of odd-position diyne components than for even-position diyne components. The simulations and STM data reveal that *shape matching of alkadiyne side chains* directs high fidelity composition variation and alignment *within 1-D tapes* that extend parallel to the monolayer's side chain direction. *Shape matching of adjacent tapes' peripheries* determines monolayer composition variation and alignment *orthogonal to the side chains*, i.e., along the monolayers' anthracene columns. The peripheries of odd-position diyne tapes support unintended packing morphologies that comprise domain breaks along the anthracene columns. The peripheries of tapes derived from even-position diyne components select the intended column packing morphology with greater fidelity, resulting in longer range order in the self-assembled monolayers.

EXPERIMENTAL METHODS

Samples for scanning tunneling microscopy were prepared by dissolving 1–2 mg of compound in 0.5 mL of phenyloctane (Aldrich, 98%). Aliquots were diluted to concentrations between 0.01 and 1.0 mM and equilibrated at the temperature of the STM room (16–20 °C). A solution drop (5 μL) was deposited on a freshly cleaved HOPG surface (ZYB grade, Momentive Performance, Strongsville, OH). STM images were acquired using a Digital Instruments NanoScope IIIa controller interfaced to a NanoScope STM. All data were collected from the solution–graphite interface using mechanically cut 80/20 Pt/Ir tips (0.25 mm, Goodfellow, Oakdale, PA) or 87/13 Pt/Rh tips (0.25 mm, Omega Engineering, Stamford, CT). The STM tip was engaged through the solution and scanned in constant height mode. After thermal drift minimized, data were collected in constant height or constant current mode with feedback parameters specified in each image. Distortions from residual thermal drift were removed by collecting and correcting consecutive pairs of up and down scans by adjusting the *x*- and *y*-thermal drift velocities to minimize differences in the two scans' unit cell parameters. STM scanner *x*- and *y*-calibration was performed prior to and during monolayer studies using sequentially captured HOPG scans (5 or 10 nm scale) corrected for thermal drift. Tip scan velocities ranged from 0.20 to 1.0 μm/s.

Molecular mechanics simulations of monolayer sections were performed using the Hyperchem[19] MM+ force field. Monolayer sections consisted of 24–36 molecules (six aryl columns, each with four to six anthracene cores) on a single graphene sheet. The graphene sheet was fixed during minimization. Partial atomic charges in molecules were determined using Mulliken population analysis of AM1 minimized structures. The termination condition for energy minimization was an rms gradient below 0.005 kcal/(Å mol). Following deletion of the graphene sheet, the monolayer section's MM+ energy was determined by a single point calculation. The adiabatic self-assembly energy (SAE) for each molecule in each morphology was calculated in two steps: first, a single point calculation was performed after a single molecule at an interior position of the monolayer section was shifted so that it no longer interacted with other molecules. The "vertical" extraction energy (VEE) of the shifted molecule was calculated as the shifted geometry's MM+ energy minus the minimized monolayer section's energy. The strain energy of the shifted molecule was determined as its MM+ energy in the monolayer minimized geometry minus its energy after minimization in isolation. The shifted molecule's adiabatic self-assembly energy (SAE) was calculated as its strain energy minus half its VEE; the factor of $^1/_2$ attributes half the stabilization energy to adjacent molecules. SAE values reported for molecules in the various packing morphologies are averages from at least four molecules.

dx.doi.org/10.1021/jp4084376 | J. Phys. Chem. B 2013, 117, 15856–15865

Chart 2

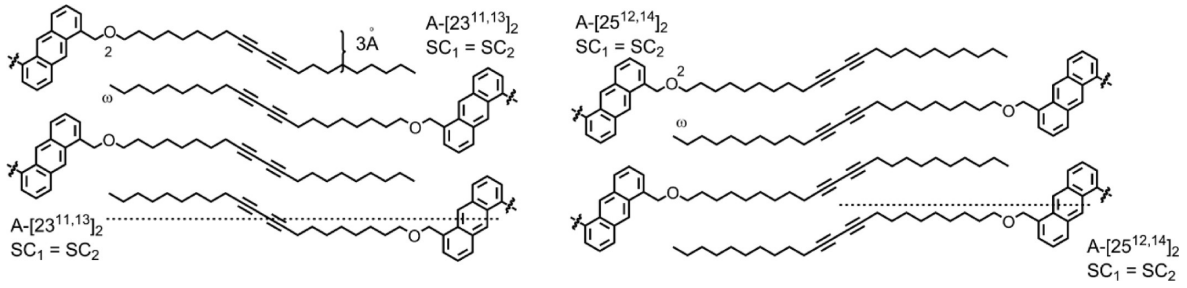

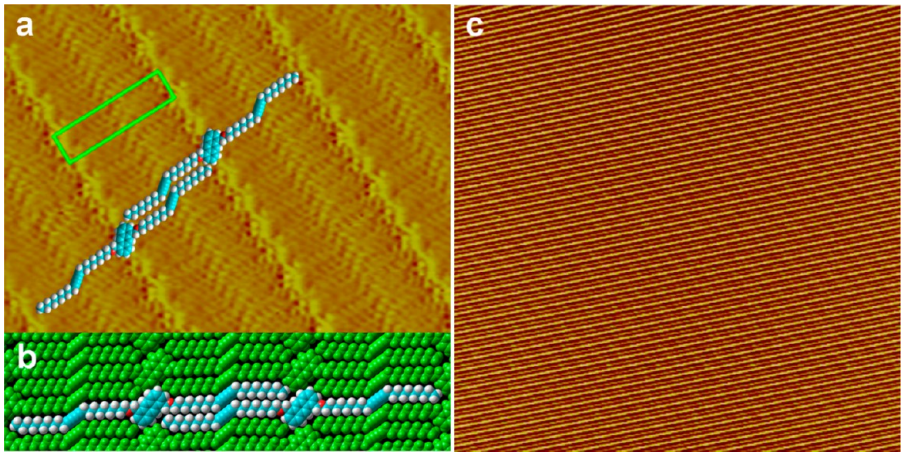

Figure 1. A-$[25^{12,14}]_2$ at the phenyloctane–HOPG interface (solution concentration, 0.2 mM): (a) constant height STM image (0.85 V, 0.1 nA, 13.6 nm × 8.0 nm) with the marked unit cell (green) and an overlay of two CPK models; (b) CPK model of the simulated monolayer; (c) constant height STM image (0.85 V, 0.1 nA, 135 nm × 135 nm).

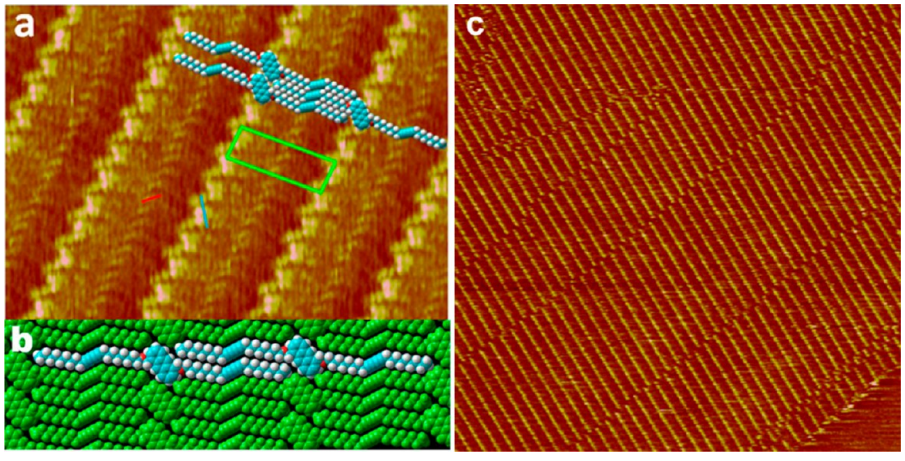

Figure 2. A-$[23^{11,13}]_2$ at the phenyloctane–HOPG interface (solution concentration, 0.4 mM): (a) constant current STM image (0.80 V, 0.1 nA, 15.3 nm × 10.9 nm) with an overlay of three CPK models, the marked unit cell (green), diyne direction (red line), and anthracene long axis (blue line); (b) CPK model of the simulated monolayer; (c) constant height STM image (0.85 V, 0.1 nA, 135 nm × 135 nm).

RESULTS AND DISCUSSION

A. Single Component, Shape Self-Complementary Diyne Monolayers. Monolayer self-assembly is driven by molecule–molecule and molecule–substrate interactions.[4−6] Planar substrates impose a bias for extensively planar conformations of physisorbed molecules.[20] The planar conformations of internal alkadiynyl chains exhibit "kinked" shapes, with a ~3 Å "vertical" offset between the two alkyl segments flanking a diyne unit (Chart 2). The kinks establish constraints on the molecular shapes that can close-pack with alkadiynyl chains in a monolayer.[21−27] In addition, the lowest energy morphologies of 1,5-(aliphatic side chain)anthracene monolayers exhibit a preference for $\omega \leftrightarrow 2$ alignment of neighboring side chains: the last heavy atom (ω) in each side chain preferentially lies in registration with the second heavy atom of both neighboring chains.[28] Assembly of stable monolayers by anthracenes bearing alkadiynyl side chains must accommodate the side chains' kinked shapes and, in the best case, establish $\omega \leftrightarrow 2$ alignment of neighboring side chains. Both criteria are satisfied by shape self-complementary alkadiynyl side chains, which have lengths of $2N + 1$ heavy

dx.doi.org/10.1021/jp4084376 | J. Phys. Chem. B 2013, 117, 15856−15865

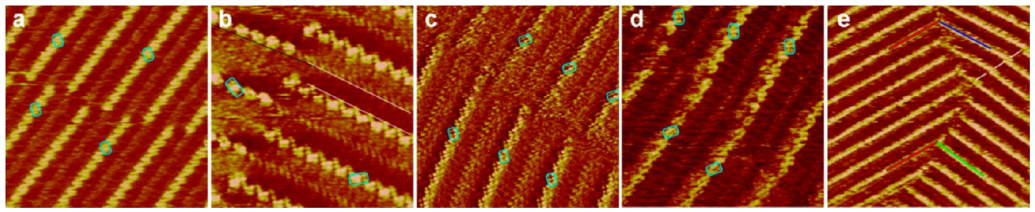

Figure 3. STM scans of domain interfaces. Cyan rectangles highlight anthracene orientations: (a) A-$[23^{11,13}]_2$ slip interface (18 nm ×18 nm); (b) A-$[23^{11,13}]_2$ enantio-slip interface (13 nm ×13 nm), where anthracene columns in the enantiotopic domains (black, white lines) are 6° off parallel; (c) A-$[29^{14,16}]_2$ offset enantio-slip interface (15 nm × 15 nm); (d) A-$[29^{14,16}]_2$ contact enantio-slip interface (15 nm × 15 nm); (e) A-$[29^{14,16}]_2$ diastereotopic 120° interfaces (50 nm × 50 nm). The red lines are parallel. The red-green angle is 115°. The red-blue angle is 124°. The broken white line marks a "contact" enantio-slip interface.

atoms and alkyne groups at the N and $N + 2$ side chain positions (Chart 2).[17] These side chains' planar conformations afford close-packing when $\omega \leftrightarrow 2$ aligned with identical alkadiynyl side chain neighbors. Anthracenes bearing two identical, shape self-complementary alkadiynyl side chains at the 1- and 5-positions readily assemble stable, single component monolayers at the solution−HOPG interface.

Submolecular resolution STM images (Figure 1a) and molecular simulations (Figure 1b) reveal the morphology of monolayers assembled by shape self-complementary A-$[25^{12,14}]_2$ (**7**) at the solution−HOPG interface. The anthracene cores assemble linear columns that border and run parallel to the $\omega \leftrightarrow 2$ aligned alkadiynyl lamellae. Stacked diyne groups form a linear band at the center of each alkadiynyl lamella, with the even position diyne group aligned nearly parallel to the anthracene long axis. The even-position diyne kink positions each side chain's inner and outer alkyl segment on the same side of a midline through the molecule, with the outer segment 3 Å further from the midline (Chart 2, right). Larger scale STM scans (e.g., Figure 1c) exhibit no disruption of the anthracene columns, the diyne columns, the lateral spacing, or the overall morphology on the 100 nm length scale. By stitching together an array of 16 100 nm × 100 nm STM scans (Figure S1 in Supporting Information), A-$[25^{12,14}]_2$ domains are found to span more than 2×10^5 nm^2 without morphology disruption. The structural elements that terminate the large domains formed by this self-complementary, even-position diyne molecule, A-$[25^{12,14}]_2$, are discussed below.

A-$[23^{11,13}]_2$ (**8**) is a shape self-complementary 1,5-bis-(alkadiynyl)anthracene derivative, with diyne groups located at odd side chain positions. The odd-position diyne group is aligned parallel to the attached anthracene's short axis and positions the side chain's outer and inner alkyl segments on opposite sides of a midline through the molecule (Chart 2, left). STM scans of A-$[23^{11,13}]_2$ monolayers (Figure 2) reveal assembly of a morphology that is similar to that of A-$[25^{12,14}]_2$ at the local level but exhibits significant differences at longer length scales. The A-$[23^{11,13}]_2$ local morphology (Figure 2a,b) consists of alternating, parallel anthracene and $\omega \leftrightarrow 2$ aligned alkadiynyl lamellae. The odd-position diynes comprise a stacked band down the center of each alkadiynyl lamella, with the diynes aligned nearly parallel to the anthracene short axis. Larger scale STM scans of A-$[23^{11,13}]_2$ monolayers display numerous breaks of the anthracene and diyne columns (Figure 2c). These breaks occur in adjacent anthracene columns spanning 100s of nanometers along directions extending nearly perpendicular to the anthracene columns and comprise interfaces between domains, with each domain exhibiting the intended local monolayer morphology throughout. Along the anthracene columns, the unit cell repeat extends only 30−50 nm before encountering a domain interface.

The disparate self-assembly fidelity along the A-$[23^{11,13}]_2$ monolayer's two unit cell axes (monolayer directions) is similar to the self-assembly behaviors exhibited by the two multi-component systems with odd-position diyne side chains, **1** and **2** and **3**−**6**; it is in stark contrast to the high fidelity of self-assembly along *both* directions of monolayers formed by the molecule with even-position diyne side chains, A-$[25^{12,14}]_2$ (**7**). These observations implicate odd-position diyne groups as structural elements that encourage domain interfaces within alkadiynylanthracene self-assembled monolayers.

B. Domain Interface Types and Areal Densities in Single Component Monolayers. Domain interfaces are the dominant defects in monolayers assembled at the solution−HOPG interface by both the odd-position and even-position alkadiynylanthracenes. Three classes of domain interfaces have been observed: (i) slip, (ii) enantio-slip, and (iii) 120°. (i) The A-$[23^{11,13}]_2$ slip interface structure (Figure 3a) aligns the diyne columns of one domain collinear with the anthracene columns of the adjacent domain. Molecules in the two domains flanking the slip interface physisorb to HOPG using the same enantiotopic face of the prochiral anthracene molecules.[29] The structure of the slip interface is robust; all observed A-$[23^{11,13}]_2$ slip interfaces exhibit this same collinear diyne to anthracene column alignment. The even-position alkadiynylanthracene monolayers do not assemble slip interfaces (vide infra). (ii) Enantio-slip interfaces arise between enantiotopic domains, i.e., domains whose anthracenes physisorb to HOPG via opposite enantiotopic faces of the prochiral anthracenes. Within A-$[23^{11,13}]_2$ monolayers, the enantio-slip interface structure is robust; the diyne columns in one domain abut the anthracene columns of the neighboring domain. Anthracene columns on opposite sides of an A-$[23^{11,13}]_2$ enantio-slip interface are slightly nonparallel, forming a $6 \pm 2°$ angle (Figure 3b). Within even-position alkadiynylanthracene monolayers, the enantio-slip interface structure is not robust. A-$[25^{12,14}]_2$ and A-$[29^{14,16}]_2$ form a number of different enantio-slip interface structures, many of which evolve during STM scanning and/or are difficult to image. These include "offset" enantio-slip interfaces (Figure 3c) in which the diyne columns of one domain abut or are proximate to anthracene columns of the enantiotopic neighboring domain, with angles of 5−9° between anthracene columns on opposite sides of the interface. A-$[25^{12,14}]_2$ and A-$[29^{14,16}]_2$ also form "contact" enantio-slip interfaces, in which nonparallel aligned anthracene columns (7−12° angle) in the two adjacent enantiotopic domains (Figure 3d) make contact. (iii) 120° interfaces form between domains oriented along different 3-fold symmetry axes of the

dx.doi.org/10.1021/jp4084376 | J. Phys. Chem. B 2013, 117, 15856−15865

HOPG (Figure 3e). 120° interfaces form between domains containing the same surface enantiomers and between enantiotopic domains. Diastereomeric 120° domain interfaces exhibit different angles between anthracene columns in flanking domains.

Areal frequencies of the three domain interface types were determined from multiple 100 nm ×100 nm sections of drop-cast monolayers (not annealed) of A-$[23^{11,13}]_2$, A-$[25^{12,14}]_2$, or A-$[29^{14,16}]_2$ (Table 1). Slip interfaces are, by far, the most common defect formed in A-$[23^{11,13}]_2$ monolayers but have not been observed in A-$[25^{12,14}]_2$ or A-$[29^{14,16}]_2$ monolayers. The high density of slip interfaces in A-$[23^{11,13}]_2$ monolayers is the primary cause of small domain widths parallel to the anthracene columns. The absence of slip interfaces in A-$[25^{12,14}]_2$ and A-$[29^{14,16}]_2$ monolayers produces longer range packing fidelity parallel to the anthracene columns.

Table 1. Areal Densities of Domain Interfaces in Drop-Cast Monolayers

	mean number of domain interfaces per 100 × 100 nm² monolayer section		
	slip	enantio-slip	120°
A-$[23^{11,13}]_2$	8.7 ± 3.2	0.7 ± 0.7	1.1 ± 0.9
A-$[25^{12,14}]_2$	0.0	0.4 ± 0.5	1.2 ± 1.0
A-$[29^{14,16}]_2$	0.0	0.9 ± 0.8	1.1 ± 0.8
A-$[23^{7,9}]_2$/A-$[23^{15,17}]_2$	0.7 ± 0.8	0.6 ± 0.7	1.0 ± 0.6
A-$[25^{10,12}]_2$/A-$[25^{14,16}]_2$	0.0	0.5 ± 0.6	1.0 ± 0.8

Diastereomeric 120° interfaces were counted in a single category as it was not possible to differentiate these interfaces at the STM scan scales employed. 120° interfaces occur with similar areal densities in monolayers formed by all three shape self-complementary alkadiynylanthracenes. They are the most common interface for the even-position diyne compounds and about one-eighth as frequent as slip interfaces for the odd-position diyne compound, A-$[23^{11,13}]_2$. Enantio-slip interfaces occur slightly less often than 120° interfaces and with remarkably similar areal densities in the odd- and even-position diyne monolayers. If interface density is controlled by thermodynamics, their areal densities should be independent of how the monolayer is prepared. Thermal annealing of drop-cast A-$[23^{11,13}]_2$ monolayers at 35 °C for up to 2 h reduced the density of slip interfaces by less than a factor of 2. Thus, A-$[23^{11,13}]_2$ monolayer samples formed by room temperature drop-casting may be nearly but not fully equilibrated. As kinetic barriers to desorption increase with chain length,[30−32] room temperature drop-cast monolayers of A-$[25^{12,14}]_2$ or A-$[29^{14,16}]_2$ are less likely than A-$[23^{11,13}]_2$ to be fully equilibrated.

C. Molecular Mechanics Simulations of Domains, Slip Interfaces, and Enantio-Slip Interfaces in Single Component Monolayers. STM scans afford well resolved images of alkadiynylanthracene packing within the domains of all monolayers and at slip and enantio-slip interfaces of A-$[23^{11,13}]_2$ monolayers. The enantio-slip interfaces of A-$[25^{12,14}]_2$ and, to a lesser extent, of A-$[29^{14,16}]_2$ appear "fuzzy", an indication of local free volume, nonoptimal packing, and dynamics at these domain interfaces.[33−36] Molecular mechanics simulations of monolayer sections on a graphene sheet were performed to model packing morphologies within domains and at interfaces and to evaluate their relative self-assembly energies (SAE).[28] The alkadiynylanthracene monolayers may be visualized as stacks of 1-D molecular tapes (Figure 4, green molecules). Each 1-D molecular tape consists of molecules in van der Waals contact at odd positions of the alkadiynyl side chains. Interactions *between side chains* determine a tape's internal composition, sequence, and alignment *parallel to the side chains*. Interactions *between tapes* determine adjacent tapes' relative alignments and sequence *along the anthracene columns*. The edge (periphery) of an odd-position diyne tape, e.g., A-$[23^{11,13}]_2$, resembles a triangle wave, with apexes at the anthracenes and the side chain 10-positions (Figure 4a). The periphery of an even-position alkadiynylanthracene tape (A-$[25^{12,14}]_2$ or A-$[29^{14,16}]_2$) resembles a trapezoid wave (Figure 4d and Figure 4g), with the side chains' outer alkyl segment comprising the plateaus and their inner alkyl segment forming the valleys. The peripheries of identical tapes are shape complementary and make close, intertape van der Waals contacts when aligned and stacked to form diyne columns and anthracene columns (Figure 4a,d,g). This alignment constitutes the "domain" morphology for both the even- and odd-position alkadiynylanthracenes.

There is a second alignment of two A-$[23^{11,13}]_2$ triangle wave tapes that affords close approach and extensive van der Waals contacts along the entirety of both tapes. This second alignment resembles a slip interface, with the diyne columns from one domain abutting and aligned collinearly with anthracene columns of the adjoining domain (Figure 4b). All odd-position, shape self-complementary alkadiynylanthracenes can access analogous slip interface structures, as their 1-D tapes have triangle wave peripheries with nearly equal spacing between the diyne and anthracene apexes. The slightly greater visibility of background near the slip interface (Figure 4b) suggests that this A-$[23^{11,13}]_2$ tape alignment provides less van der Waals stabilization than the domain alignment.

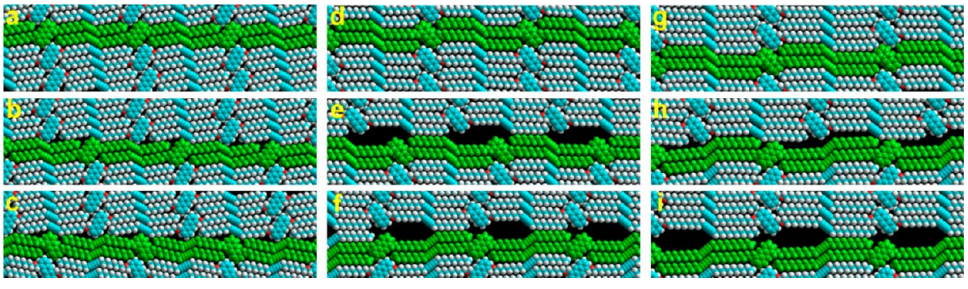

Figure 4. CPK models of molecular mechanics (MM+) minimized monolayer sections on graphene: A-$[23^{11,13}]_2$ (a) domain, (b) slip interface, and (c) enantio-slip interface sections; A-$[25^{12,14}]_2$ (d) domain, (e) slip interface, and (f) contact enantio-slip interface sections; A-$[29^{14,16}]_2$ (g) domain, (h) offset enantio-slip interface, and (i) contact enantio-slip interface sections.

dx.doi.org/10.1021/jp4084376 | J. Phys. Chem. B 2013, 117, 15856−15865

Table 2. Self-Assembly Energy and Estimated Density of Alkadiynylanthracenes Tape Alignments

	self-assembly energy (kcal/mol)//no. per 100 nm		
	domain	slip	enantio-slip
A-$[23^{11,13}]_2$	−34.7//88	−33.7//16	−31.9//1
A-$[25^{12,14}]_2$	−38.2//104	−32.7//0	−31.9, −32.3//0, 0
A-$[29^{14,16}]_2$	−45.3//104	−38.8//0	−38.2, −38.9//0, 0
A-$[23^{7,9}]_2$/A-$[23^{15,17}]_2$	−34.5/−34.9//103	−29.0/−34.7//1	
A-$[25^{10,12}]_2$/A-$[25^{14,16}]_2$	−38.3/−38.1//- - -		

This second tape alignment is not favorable for even-position, shape self-complementary alkadiynylanthracenes (Figure 4e). The trapezoid wave peripheries of adjacent A-$[25^{12,14}]_2$ tapes cannot form close van der Waals contact along their entire peripheries where aligned in analogy to a slip interface. Although solvent molecule adsorption at these gaps may mitigate the loss of tape stabilization,[37,38] the peripheries of even-position alkadiynylanthracene tapes are much less suited to assemble stable slip interfaces than are odd-position alkadiynylanthracene tapes. This explains why slip interfaces are readily observed within A-$[23^{11,13}]_2$ monolayers but have not been observed in STM scans of A-$[25^{12,14}]_2$ or A-$[29^{14,16}]_2$ monolayers.

The triangle wave peripheries of two enantiotopic A-$[23^{11,13}]_2$ tapes produce moderate van der Waals contacts in alignments reminiscent of enantio-slip interfaces (Figure 4c), with the anthracene columns in one domain abutting and aligned nonparallel with the diyne columns of the adjacent enantiotopic domain. In this model, the tapes at the enantio-slip interface do not pack as closely as tapes at a slip interface or in the domain morphology, suggesting enantio-slip interfaces will have higher energy and should occur less frequently than slip interfaces within equilibrated A-$[23^{11,13}]_2$ monolayers. All odd-position, shape self-complementary alkadiynylanthracenes can assemble similar enantio-slip interface structures.

The trapezoid wave peripheries of even-position alkadiyne tapes fail to provide close packing along the peripheries of adjacent, enantiotopic tapes (Figure 4f,h,i). Both A-$[25^{12,14}]_2$ and A-$[29^{14,16}]_2$ have multiple alignments of two enantiotopic, even-position tapes that afford similarly poor van der Waals contacts along the tapes' peripheries (vide infra). Polymorphism may contribute to the higher densities of enantio-slip interfaces compared to slip interfaces within even-position alkadiynylanthracene monolayers.

The molecular mechanics simulated monolayer sections were used to estimate a self-assembly energy (SAE) for each compound in its domain, slip, and enantio-slip tape alignment. The self-assembly energy includes interactions between alkadiynylanthracenes but neglects interactions with solvent or the underlying graphene sheet. Not surprisingly, the domain alignment of each compound generates the most negative self-assembly energy (Table 2), as this tape alignment provides more extensive van der Waals contacts than do the slip and enantio-slip alignments. For A-$[23^{11,13}]_2$, the SAE of the slip and enantio-slip alignments are 1.0 and 2.8 kcal/mol higher in energy than the domain alignment, respectively. For the even-position A-$[25^{12,14}]_2$ and A-$[29^{14,16}]_2$ monolayers, the domain alignments are at least 5.5 kcal/mol more stable than the corresponding slip, offset enantio-slip, and contact enantio-slip alignments.

The SAE values were used to estimate densities of domain, slip, and enantio-slip tape alignments per 100 nm monolayer section (104 tape interfaces). This Boltzmann estimate ignores 120° interfaces, presumes all tape alignments have identical entropy of formation and that graphene and solvent do not impact the relative assembly free energies (see Supporting Information). The SAE based estimates of A-$[23^{11,13}]_2$ slip and enantio-slip interface densities (Table 2) agree to within a factor of 2 with the measured values (Table 1). For A-$[25^{12,14}]_2$ and A-$[29^{14,16}]_2$ monolayers, the simulation SAE values predict that slip interfaces and enantio-slip interfaces lie at energies too high to assemble measurable densities. The slip interface density predictions for A-$[25^{12,14}]_2$ and A-$[29^{14,16}]_2$ agree with the experimental results (none detected) but the predicted enantio-slip densities ($<10^{-5}$/100 nm) underestimate the experimental results by 5 orders of magnitude (Table 1). For these two molecules, the thermodynamic (simulation) estimates of enantio-slip densities must incorporate incorrect assumptions. It is possible that solvent participates in the assembly, and stabilization, of particular enantio-slip interface structures. Alternatively, the various enantio-slip interfaces formed by even-position diyne monolayers may arise primarily through collision of independently nucleated and growing enantiotopic domains. Although these even-position diyne molecules lack a thermodynamically favorable structure that can stabilize the enantio-slip interface, they also lack a kinetically viable path for eliminating the interface,[38] as this requires flipping all molecules in one of the domains. Random nucleation of enantiotopic domains explains the observation of comparable enantio-slip interface areal densities in all three single-component (also in the two-component) monolayers (Table 1) despite the vastly different SAE predictions. If enantio-slip interface formation is random, the good agreement between observed and predicted enantio-slip interface areal densities for A-$[23^{11,13}]_2$ may be fortuitous. Statistical nucleation of domains may also explain the observation of similar areal densities for 120° interfaces in all five monolayer systems.

D. Domain Interfaces and Areal Densities in Shape Selective Two-Component Monolayer Systems. The above studies identified odd-position diyne groups as structural elements that increase the density of slip interfaces along the anthracene columns. Those studies did not ascertain whether multicomponent systems also increase the densities of domain interfaces within self-assembled alkadiynylanthracene monolayers. Within one-component alkadiynylanthracene monolayers, the shape matching criterion constrains the diyne group to the center of the side chain and thus to the center of each 1-D tape's aliphatic sections. This constraint is removed for monolayers assembled from pairwise, shape complementary alkadiynylanthracene components. Shape complementary, even-position diyne components will still assemble 1-D tapes with trapezoid wave peripheries. However, the widths and spacings between the plateaus and valleys along the tape periphery will change significantly with diyne location and side chain length. Similarly, shape matched odd-position diyne

dx.doi.org/10.1021/jp4084376 | J. Phys. Chem. B 2013, 117, 15856−15865

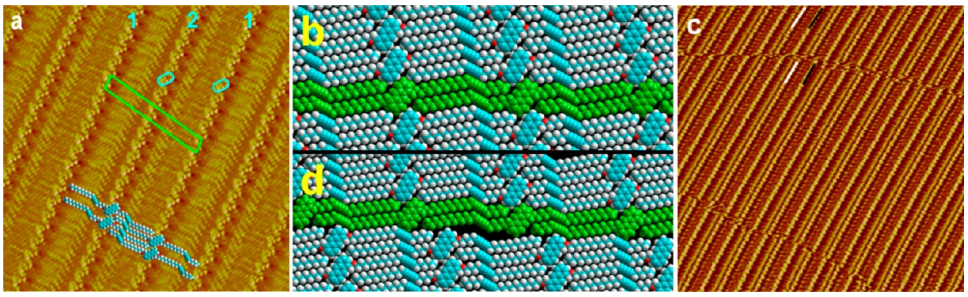

Figure 5. A-$[23^{7,9}]_2$/A-$[23^{15,17}]_2$ at the phenyloctane–HOPG interface (solution concentration, 0.4 mM): (a) constant height STM image (0.8 V, 0.1 nA, 18 nm × 18 nm) with CPK overlays and unit cell (green box); (b) CPK model of the simulated monolayer, where the molecules in a two-component tape are shaded green; (c) constant height STM image (1.0 V, 0.1 nA, 60 nm × 60 nm) showing two slip interfaces. The black bars mark anthracenes in A-$[23^{15,17}]_2$ (**1**) columns. The white bars mark anthracenes in A-$[23^{7,9}]_2$ (**2**) columns. The A-$[23^{15,17}]_2$ anthracene columns (black) align with every second diyne column across the slip interface. The diyne column to the right of each A-$[23^{7,9}]_2$ column is faint. (d) CPK model of the minimized A-$[23^{7,9}]_2$/A-$[23^{15,17}]_2$ interface.

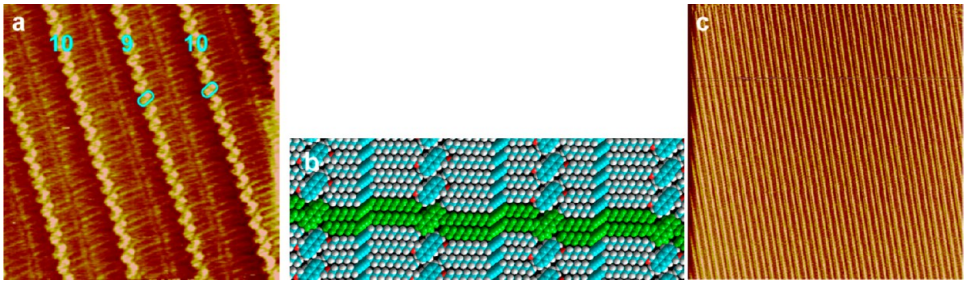

Figure 6. A-$[25^{10,12}]_2$/A-$[25^{14,16}]_2$ at the phenyloctane–HOPG interface: (a) constant height STM image (0.85 V, 0.1 nA, 15 nm × 15 nm, 0.3 mM); (b) CPK model of the minimized monolayer, where the molecules in a two-component tape are shaded green and the diyne columns are closer to the anthracene columns of A-$[25^{10,12}]_2$; (c) larger scale image showing a typical, interface free domain (0.80 V, 0.1 nA, 150 nm × 150 nm, 0.25 mM).

components will assemble 1-D tapes with triangle wave peripheries but with sets of spacings between apexes that depend on diyne location and side chain length. Consequently, the tapes assembled by each shape complementary side chain pair may exhibit different proclivities for slip and enantio-slip interface assembly. For this investigation, the even-position components' diyne groups were shifted by the smallest possible amount (two side chain positions) from side chain center (A-$[25^{10,12}]_2$/A-$[25^{14,16}]_2$) whereas the odd-position components' diyne groups were shifted slightly more (four side chain positions) from side chain center (A-$[23^{7,9}]_2$/A-$[23^{15,17}]_2$).

The complementary, kink-shaped alkadiynyl side chains of the A-$[23^{7,9}]_2$/A-$[23^{15,17}]_2$ pair drive composition alternation within their two component monolayer (Figure 5a).[17] The unit cell contains one copy of each molecule. The diynes are aligned parallel to the anthracene short axis and form linear stacks that are closer to the A-$[23^{7,9}]_2$ anthracene columns. The diynes within each stack arise, alternately, from the two different, shape complementary side chains (Figure 5b). At longer length scales, the drop-cast monolayers assembled by this odd-position alkadiynylanthracene pair exhibit slip interfaces (Figure 5c), enantio-slip interfaces, and 120° interfaces. Slip interfaces aligned roughly perpendicular to the anthracene columns position all A-$[23^{15,17}]_2$ anthracene columns in one domain collinear with every second diyne column of the domain across the slip interface (Figure 5c). STM scans did not produce well resolved images near enantio-slip interfaces, although a few scans appear to align A-$[23^{15,17}]_2$ anthracene columns in each domain noncollinearly with every second diyne column of the adjoining enantiotopic domain. The areal density of slip interfaces determined from 100 nm × 100 nm scans of A-$[23^{7,9}]_2$/A-$[23^{15,17}]_2$ monolayers (Table 1) is 1 order of magnitude smaller than the slip interface density in the single component A-$[23^{11,12}]_2$ monolayers. By contrast, areal densities of enantio-slip and 120° interfaces within A-$[23^{7,9}]_2$/A-$[23^{15,17}]_2$ monolayers are comparable to the corresponding interfaces densities in single component monolayers.

The shape complementary alkdiynyl side chains of the A-$[25^{10,12}]_2$/A-$[25^{14,16}]_2$ pair also drive composition alternation along the side chain axis of the mixed monolayer (Figure 6a). The diynes assemble linear stacks extending parallel to and positioned slightly closer to the anthracene columns assembled from A-$[25^{10,12}]_2$. The diynes within each stack alternately belong to the two different side chains (Figure 6b). The two-component, 1-D tapes exhibit a trapezoid wave periphery. Large sections of the A-$[25^{10,12}]_2$/A-$[25^{14,16}]_2$ mixed monolayer (Figure 6c) lack domain interfaces: slip interfaces have not been identified in any STM images of this two-component monolayer, and the areal densities of enantio-slip and 120° interfaces are comparable to those observed in the four other monolayer systems described in this study (Table 1). This two-component, even-position diyne monolayer exhibits (i) high fidelity composition alternation and alignment within its 1-D tapes and (ii) greater alignment fidelity along the anthracene columns than the A-$[23^{7,9}]_2$/A-$[23^{15,17}]_2$ monolayers and alignment fidelity that is comparable to that observed within the single component, even-position diyne monolayers formed by A-$[25^{12,14}]_2$ and A-$[29^{14,16}]_2$.

Analysis of the interface statistics reveals that stacking of odd-diyne-position A-$[23^{7,9}]_2$/A-$[23^{15,17}]_2$ tapes allows but does not favor slip interface assembly, whereas stacking of even-diyne-position A-$[25^{10,12}]_2$/A-$[25^{14,16}]_2$ tapes does not support slip

dx.doi.org/10.1021/jp4084376 | J. Phys. Chem. B 2013, 117, 15856–15865

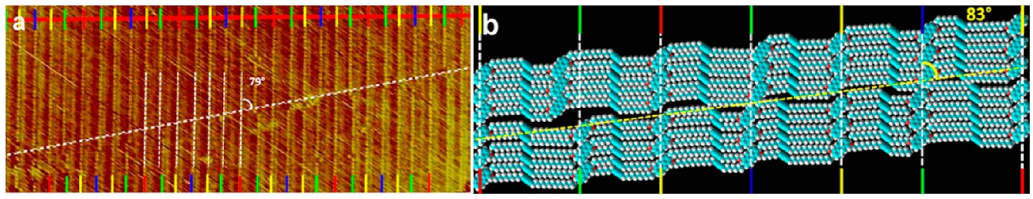

Figure 7. (a) STM scan displaying the slip interface region of a four-component monolayer assembled from odd-position alkadiynyl anthracenes. The anthracene column compositions on opposite sides of the interface are coded using four different color bars. The vertical dashed white lines indicate the anthracene column locations in the upper domain. (b) CPK model of the four-component monolayer's slip interface region. The vertical dashed white lines connecting red with yellow color bars or yellow with yellow color bars on opposite sides of the interface region overlay undisrupted anthracene columns. The dashed white lines connecting blue with green color bars overlay columns with small anthracene displacements. The dashed white lines connecting green with green color bars overlay columns with larger and opposite direction anthracene displacements.

interface formation. These results show that multicomponent systems do not necessarily increase domain interface densities. If anything, increasing the number of components decreases slip interface density within odd-position diyne monolayers. It is remarkable that neither the number of components in the monolayer system (one or two) nor the diyne position within the side chain (odd or even) significantly alters the densities of the enantio-slip interfaces or of 120° interfaces. These observations are consistent with the domain nucleation rationale for these interfaces' densities.[38]

Molecular mechanics simulations were performed for the domain morphologies of both two-component monolayers and for the slip interface structures of A-$[23^{7,9}]_2$/A-$[23^{15,17}]_2$ (Figure 5d). Insufficient STM structural characterization was available for A-$[23^{7,9}]_2$/A-$[23^{15,17}]_2$ enantio-slip interfaces or for A-$[25^{10,12}]_2$/A-$[25^{14,16}]_2$ slip or enantio-slip interface structures to allow meaningful simulation and SAE value determinations. The domain structure SAE values for A-$[23^{7,9}]_2$ and A-$[23^{15,17}]_2$ are similar to each other, −34.5 and −34.9 kcal/mol, respectively, and to the SAE value of A-$[23^{11,12}]_2$. For a slip-interface propagating perpendicular to the anthracene columns (Figure 5d), A-$[23^{7,9}]_2$ loses more van der Waals contacts than A-$[23^{15,17}]_2$ (Table 2). The average SAE value for this slip interface structure, −31.9 kcal/mol, indicates that the slip alignment is 2.8 kcal/mol less stable than the domain alignment average SAE, −34.7 kcal/mol. A Boltzmann estimate predicts that the slip interface density in A-$[23^{7,9}]_2$/A-$[23^{15,17}]_2$ monolayers is an order of magnitude lower than in A-$[23^{11,12}]_2$ monolayers, in reasonable agreement with experiment (Tables 1 and 2). As no detailed structural characterization of curved slip interfaces or of enantio-slip interfaces was obtained, SAE determinations of these structures were not attempted. The structures of these and the 120° interfaces remain open questions.

E. Slip Interfaces in a Four-Component Monolayer. The previously reported four-component alkadiynylanthracene system assembled monolayers with high fidelity packing along the side chain direction.[18] These monolayers contained enantiopic interfaces and "column defects" that occurred systematically along a line running at a 80 ± 5° angle relative to the anthracene columns (Figure 7a). The six molecule unit cells (repeat pattern along the side chain axis) on opposite sides of the defect line were displaced by two anthracene columns. In light of the current study's identification of correlated anthracene column displacements as slip interfaces, efforts were made to model the systematic defects of the four-component system. Figure 7b presents a CPK model of a slip interface that generates a two-column relative displacement of the unit cells on opposite sides of the interface and a "defect propagation line" that runs at 83° relative to the anthracene columns. The model also matches the experimental STM observations that (i) every other anthracene column crosses the "defect propagation line" without disruption and (ii) the disrupted anthracene columns alternate in the direction and magnitude of the column displacement. The model is interesting because the last tape in each domains consists of diyne molecules in contact via their side chains' even positions. This tape has a trapezoidal periphery that is slanted relative to (not perpendicular to) the anthracene columns. These interface tapes contrast with the 1-D tape structures invoked to explain the abundance of slip interfaces in odd-position diyne monolayers, which have triangle wave peripheries and molecules making contact via the side chain odd positions. Both tape descriptions are equally valid, and both are useful for explaining structural characteristics of the monolayers. It is possible that the curved interfaces mentioned above might be reproduced using 1-D tapes incorporating various fractions of side chain contacts at odd and even positions.

■ CONCLUSIONS

Shape complementary, kinked alkadiyne side chains are useful for directing self-assembly of multicomponent 1,5-substituted anthracene monolayers with designed compositional variation along one direction (1-D patterned monolayers). In drop-cast monolayers, the1-D patterns persist for 100s of nanometers along the side chain direction, driven by optimal van der Waals interactions among shaped matched side chain pairs. The 1-D patterns terminate at interfaces between domains whose side chains are oriented along different 3-fold symmetry axes of the underlying graphite surface (120° interfaces). No compositional variation is intended along the orthogonal monolayer direction, which is nearly parallel to the monolayer's anthracene columns. Three domain interfaces terminate the anthracene columns: 120° interfaces, slip interfaces, and enantio-slip interfaces. For anthracenes with diynes in odd side chain positions, slip interfaces are the most abundant column terminating domain interface. Slip interfaces are not observed in monolayers assembled by anthracenes with diynes in even side chain positions. 120° interfaces and enantio-slip interfaces terminate anthracene columns to similar extents in both one- and two-component monolayers assembled by molecules with either odd- or even-position diyne side chains. Consequently, the mean domain size along the anthracene column direction is significantly smaller in monolayers assembled from odd-position diyne side chain molecules than in monolayers assembled from even-position diyne side chain molecules.

dx.doi.org/10.1021/jp4084376 | J. Phys. Chem. B 2013, 117, 15856−15865

For the purpose of understanding domain interfaces and polymorphism, one can visualize 1,5-alkadiynyl anthracene monolayers as stacks of 1-D molecular tapes. 1-D tapes formed from molecules bearing odd-position diyne side chains have triangle wave peripheries. There are two alignments of adjacent odd-position tapes that afford van der Waals contacts and tape−tape interactions that are comparable to the preferred, domain alignment. Thermal accessibility of these alternate tape alignments produces frequent domain boundaries. 1-D tapes formed from even-position diyne side chain molecules have trapezoid wave peripheries. Only the domain tape alignment is thermodynamically accessible. Slip tape alignments and the corresponding slip interfaces are not observed in even-position diyne monolayers. The results demonstrate the necessity of designing selectivity into molecule−molecule (0 D) and tape−tape (1 D) contacts to produce large individual domains in these types of multicomponent 2 D assemblies.

Despite having very high energies, enantio-slip interfaces are observed in even-position diyne monolayers. STM image resolution at these enantiotopic interfaces is poor, consistent with rapid dynamics arising from loose packing of adjacent, trapezoid-wave periphery tapes. Enantio-slip, 120°, and slip interfaces can arise through contact of separately nucleated and growing domains. A number of observations suggest that domain collisions and kinetics influence the morphologies of these drop-cast monolayers. (i) Annealing at slightly elevated temperatures reduces slip interface density in A-$[23^{11,13}]_2$ monolayers. (ii) Enantio-slip interfaces form with comparable areal densities in one- and two-component monolayers assembled from odd- or even-position diynes despite calculations indicating vastly different interface energies. Identical rates of enantiotopic domain nucleation and growth and the absence of kinetically competent processes to resolve enantio-slip interfaces/enantiotopic domains[38] provide an explanation for their persistence despite high energetic cost. (iii) 120° interfaces form with similar areal densities in all monolayer systems studied. Identical rates of domain nucleation and growth aligned along different graphite symmetry axes and the absence of kinetically competent processes to resolve the interfaces can explain these observations. The similar areal densities of structurally unrelated enantio-slip and 120° interfaces in all five diyne monolayer systems would require an interesting thermodynamic explanation. As monolayer assembly kinetics, including intrinsically slow rates of interface resolution, appear to limit domain size, future efforts to produce even larger single domains will require strategies that modulate nucleation and/or growth kinetics differentially for enantiotopic[39] and 120° rotated domains.[40]

■ ASSOCIATED CONTENT

Supporting Information

Synthetic methods and spectral data for all new compounds, a stitched image of an A-$[25^{12,14}]_2$ domain generated from 16 100 nm × 100 nm STM scans, and Boltzmann model used to estimate tape alignment densities. This material is available free of charge via the Internet at http://pubs.acs.org.

■ AUTHOR INFORMATION

Present Addresses

[†]Y.X.: Department of Materials Science and Engineering, University of California—Berkeley, Berkeley, CA, 94720-1760.

[‡]T.P.: Faculty of Biomedical Engineering, Czech Technical University, 272 01 Kladno, Czech Republic.

Notes

The authors declare no competing financial interest.

■ ACKNOWLEDGMENTS

The authors thank the National Science Foundation (Grant CHE1058241) for support of this work.

■ REFERENCES

(1) Kushner, D. J. Self-Assembly of Biological Structures. *Bacteriol. Rev.* **1969**, *33*, 302−345.

(2) Saranathan, V.; Forster, J. D.; Noh, H.; Liew, S.-F.; Mochrie, S. G. J.; Cao, H.; Dufresne, E. R.; Prum, R. O. Structure and Optical Function of Amorphous Photonic Nanostructures from Avian Feather Barbs: A Comparative Small Angle X-ray Scattering (SAXS) Analysis of 230 Bird Species. *J. R. Soc. Interface* **2012**, *9*, 2563−2580.

(3) Ban, N.; Nissen, P.; Hansen, J.; Moore, P. B.; Steitz, T. A. The Complete Atomic Structure of the Large Ribosomal Subunit at 2.4 Å Resolution. *Science* **2000**, *289*, 905−920.

(4) Mali, K. S.; Adisoejoso, J.; Ghijsens, E.; De Cat, I.; De Feyter, S. Exploring the Complexity of Supramolecular Interactions for Patterning at the Liquid−Solid Interface. *Acc. Chem. Res.* **2012**, *45*, 1309−1320.

(5) Cardenas, L.; Lipton-Duffin, J.; Rosei, F. Transformations of Molecular Frameworks by Host−Guest Response: Novel Routes toward Two-Dimensional Self-Assembly at the Solid−Liquid Interface. *Jpn. J. Appl. Phys.* **2011**, *50*, 08LA021−08LA026.

(6) Ciesielski, A.; Palma, C.-A.; Bonini, M.; Samori, P. Towards Supramolecular Engineering of Functional Nanomaterials: Pre-Programming Multi-Component 2D Self-Assembly at Solid−Liquid Interfaces. *Adv. Mater.* **2010**, *22*, 3506−3520.

(7) Rabe, J. P.; Buchholz, S. Commensurability and Mobility in Two-Dimensional Molecular Patterns on Graphite. *Science* **1991**, *253*, 424−427.

(8) Müller, H.; Petersen, J.; Strohmaier, R.; Gompf, B.; Eisenmenger, W.; Vollmer, M. S.; Effenberger, F. Influence of Polar Substituents on the Epitaxy of Oligothiophenes on Graphite: A Systematic STM Investigation. *Adv. Mater.* **1996**, *8*, 733−737.

(9) Surin, M.; Samori, P. Multicomponent Monolayer Architectures at the Solid−Liquid Interface: Towards Controlled Space-Confined Properties and Reactivity of Functional Building Blocks. *Small* **2007**, *3*, 190−194.

(10) Northrop, B. H.; Zheng, Y.-R.; Chi, K.-W.; Stang, P. J. Self-Organization in Coordination-Driven Self-Assembly. *Acc. Chem. Res.* **2009**, *42*, 1554−1563.

(11) Wei, Y.; Tong, W.; Zimmt, M. B. Self-Assembly of Patterned Monolayers with Nanometer Features: Molecular Selection Based on Dipole Interactions and Chain Length. *J. Am. Chem. Soc.* **2008**, *130*, 3399−3405.

(12) Llanes-Pallas, A.; Matena, M.; Jung, T.; Prato, M.; Stöhr, M.; Bonifazi, D. Trimodular Engineering of Linear Supramolecular Miniatures on Ag(111) Surfaces Controlled by Complementary Triple Hydrogen Bonds. *Angew. Chem., Int. Ed.* **2008**, *47*, 7726−7730.

(13) Lei, S.; Surin, M.; Tahara, K.; Adisoejoso, J.; Lazzaroni, R.; Tobe, Y.; De Feyter, S. Programmable Hierarchical Three-Component 2D Assembly at a Liquid−Solid Interface: Recognition, Selection, and Transformation. *Nano Lett.* **2008**, *8*, 2541−2546.

(14) Silly, F.; Shaw, A. Q.; Porfyrakis, K.; Warner, J. H.; Watt, A. A. R.; Castell, M. R.; Umemoto, H.; Akachi, T.; Shinoharad, H.; Briggs, G. A. D. Grating of Single Lu@C_{82} Molecules Using Supramolecular Network. *Chem. Commun.* **2008**, 4616−4618.

(15) Adisoejoso, J.; Tahara, K.; Okuhata, S.; Lei, S.; Tobe, Y.; De Feyter, S. Two-Dimensional Crystal Engineering: A Four-Component Architecture at a Liquid−Solid Interface. *Angew. Chem., Int. Ed.* **2009**, *48*, 7353−7357.

(16) Le, J. D.; Pinto, Y.; Seeman, N. C.; Musier-Forsyth, K.; Taton, T. A.; Kiehl, R. A. DNA-Templated Self-Assembly of Metallic Nanocomponent Arrays on a Surface. *Nano Lett.* **2004**, *4*, 2343−2347.
(17) Xue, Y.; Zimmt, M. B. Tetris in monolayers: patterned self-assembly using side chain shape. *Chem. Commun.* **2011**, *47*, 8832−8834.
(18) Xue, Y.; Zimmt, M. B. Patterned Monolayer Self-Assembly Programmed by Side Chain Shape: Four-Component Gratings. *J. Am. Chem. Soc.* **2012**, *134*, 4513−4516.
(19) *HyperChem Professional 8.0*; Hypercube, Inc. (1115 NW 4th Street, Gainesville, FL 32601, USA).
(20) Malah, T. E.; Ciesielski, A.; Piot, L.; Troyanov, S. I.; Mueller, U.; Weidner, S.; Samori, P.; Hecht, S. Conformationally Pre-Organized and pH-Responsive Flat Dendrons: Synthesis and Self-Assembly at the Liquid−Solid Interface. *Nanoscale* **2012**, *4*, 467−472.
(21) Okawa, Y.; Aono, M. Nanoscale Control of Chain Polymerization. *Nature* **2001**, *409*, 683−684.
(22) Takajo, D.; Okawa, Y.; Hasegawa, T.; Aono, M. Chain Polymerization of Diacetylene Compound Multilayer Films on the Topmost Surface Initiated by a Scanning Tunneling Microscope Tip. *Langmuir* **2007**, *23*, 5247−5250.
(23) Endo, O.; Furuta, T.; Ozaki, H.; Sonoyama, M.; Mazaki, Y. Structures of 17,19-Hexatriacontadiyne Monolayers on Au(111) Studied by Infrared Reflection Absorption Spectroscopy and Scanning Tunneling Microscopy. *J. Phys. Chem. B* **2006**, *110*, 13100−13106.
(24) Sullivan, S. P.; Schnieders, A.; Mbugua, S. K.; Beebe, T. P. Controlled Polymerization of Substituted Diacetylene Self-Organized Monolayers in Molecule Corrals. *Langmuir* **2005**, *21*, 1322−1327.
(25) Ozaki, H.; Funaki, T.; Mazaki, Y.; Masuda, S.; Harada, Y. Single Sheet of a Quasi-Planar Macromolecule Prepared by Photopolymerization at a Solid Surface. *J. Am. Chem. Soc.* **1995**, *117*, 5596−5597.
(26) Miura, A.; De Feyter, S.; Abdel-Mottaleb, M. M. S.; Gesquière, A.; Grim, P. C. M.; Moessner, G.; Sieffert, M.; Klapper, M.; Müllen, K.; De Schryver, F. C. Light- and STM-Tip-Induced Formation of One-Dimensional and Two-Dimensional Organic Nanostructures. *Langmuir* **2003**, *19*, 6474−6482.
(27) Mali, K. S.; Van Averbeke, B.; Bhinde, T.; Brewer, A. Y.; Arnold, T.; Lazzaroni, R.; Clarke, S. M.; De Feyter, S. To Mix or Not To Mix: 2D Crystallization and Mixing Behavior of Saturated and Unsaturated Aliphatic Primary Amides. *ACS Nano* **2011**, *5*, 9122−9137.
(28) Tong, W.; Wei, X.; Zimmt, M. B. Dipolar Control of Monolayer Morphology on Graphite: Self-Assembly of Antracenes with Odd Length Diether Side Chains. *J. Phys. Chem. C.* **2009**, *113*, 17104−17113.
(29) Wei, Y.; Kannappan, K.; Flynn, G. W.; Zimmt, M. B. Scanning Tunneling Microscopy of Prochiral Anthracene Derivatives on Graphite: Chain Length Effects on Monolayer Morphology. *J. Am. Chem. Soc.* **2004**, *126*, 5318−5322.
(30) Stevens, F.; Beebe, T. P., Jr. Dynamical Exchange Behavior in Organic Monolayers Studied by STM Analysis of Labeled Mixtures. *Langmuir* **1999**, *15*, 6884−6889.
(31) Padowitz, D. F.; Sada, D. M.; Kemer, E. L.; Dougan, M. L.; Xue, W. A. Molecular Tracer Dynamics in Crystalline Organic Films at the Solid−Liquid Interface. *J. Phys. Chem. B.* **2002**, *106*, 593−598.
(32) Piot, L.; Marchenko, A.; Wu. J. Müllen, K.; Fichou, D. Structural Evolution of Hexa-*peri*-hexabenzocoronene Adlayers in Heteroepitaxy on *n*-Pentacontane Template Monolayers. *J. Am. Chem. Soc.* **2005**, *127*, 16245−16250.
(33) Rabe, J. P.; Buchholz, S. Direct Observation of Molecular Structure and Dynamics at the Interface Between a Solid Wall and an Organic Solution by Scanning Tunneling Microscopy. *Phys. Rev. Lett.* **1991**, *66*, 2096−2099.
(34) Hibino, M.; Sumi, A.; Hatta, I. Molecular Motion at Domain Boundaries in Fatty Acid Monolayers on Graphite Observed by Scanning Tunneling Microscopy. *Thin Solid Films* **1996**, *273*, 272−278.
(35) Stabel, A.; Heinz, R.; Rabe, J. P.; Wegner, G.; De Schryver, F. C.; Corens, D.; Dehaen, W.; Süling, C. STM Investigation of 2D Crystals of Anthrone Derivatives on Graphite: Analysis of Molecular Structure and Dynamics. *J. Phys. Chem.* **1995**, *99*, 8690−8697.
(36) Stabel, A.; Heinz, R.; De Schryver, F. C.; Rabe, J. P. Ostwald Ripening of Two-Dimensional Crystals at the Solid−Liquid Interface. *J. Phys. Chem.* **1995**, *99*, 505−507.
(37) Gesquière, A.; Abdel-Mottaleb, M. M.; De Feyter, S.; De Schryver, F. C.; Sieffert, M.; Müllen, K.; Calderone, A.; Lazzaroni, R.; Brédas, J. Dynamics in Physisobred Monolayers of 5-Alkoxy-isophthalic Acid Derivatives at the Liquid/Solid Interface Investigated by Scanning Tunneling Microscopy. *Chem.—Eur. J.* **2000**, *6*, 3739−3746.
(38) Florio, G. M.; Klare, J. E.; Pasamba, M. O.; Werblowsky, T. L.; Hyers, M.; Berne, B. J.; Hybertsen, M. S.; Nuckolls, C.; Flynn, G. W. Frustrated Ostwald Ripening in Self-Assembled Monolayers in Cruciform π-Systems. *Langmuir* **2006**, *22*, 10003−10008.
(39) Katsonis, N.; Xu, H.; Haak, R. M.; Kudernac, T.; Tomovic, Z.; George, S.; Van der Auweraer, M.; Schenning, A. P. H. J.; Meijer, E. W.; Feringa, B. L.; et al. Emerging Solvent-Induced Homochirality by the Confinement of Achiral Molecules against a Solid Surface. *Angew. Chem., Int. Ed.* **2008**, *47*, 4997−5001.
(40) Lee, S.-L.; Chi, C.-Y. J.; Huang, M.-J.; Chen, C.-h.; Li, C.-W.; Pati, K.; Liu, R.-S. Shear-Induced Long-Range Uniaxial Assembly of Polyaromatic Monolayers at Molecular Resolution. *J. Am. Chem. Soc.* **2008**, *130*, 10454−10455.